

An Efficient Quantum Readout Error Mitigation for Sparse Measurement Outcomes of Near-term Quantum Devices

Bo Yang¹, Rudy Raymond^{2,3}, and Shumpei Uno^{3,4}

¹*Graduate School of Information Science and Technology,*

The University of Tokyo, Bunkyo-ku, Tokyo 113-8656, Japan

²*IBM Quantum, IBM Research-Tokyo, 19-21 Nihonbashi Hakozaiki-cho, Chuo-ku, Tokyo, 103-8510, Japan*

³*Quantum Computing Center, Keio University, Hiyoshi 3-14-1, Kohoku-ku, Yokohama 223-8522, Japan*

⁴*Mizuho Research & Technologies, Ltd, 2-3 Kanda-Nishikicho, Chiyoda-ku, Tokyo, 101-8443, Japan*

(Dated: February 21, 2022)

The readout error on the near-term quantum devices is one of the dominant noise factors, which can be mitigated by classical post-processing called quantum readout error mitigation (QREM). The standard QREM method applies the inverse of noise calibration matrix to the outcome probability distribution using exponential computational resources to the system size. Hence this standard approach is not applicable to the current quantum devices with tens of qubits and more. We propose two efficient QREM methods on such devices whose computational complexity is $O(ns^2)$ for probability distributions on measuring n qubits with s shots. The main targets of the proposed methods are the sparse probability distributions where only a few states are dominant. We compare the proposed methods with several recent QREM methods on the following three cases: expectation values of GHZ state, its fidelities, and the estimation error of maximum likelihood amplitude estimation (MLAE) algorithm with modified Grover iterator. The two cases of the GHZ state are on real IBM quantum devices, while the third is by numerical simulation. The proposed methods can be applied to mitigate GHZ states up to 65 qubits on IBM Quantum devices within a few seconds to confirm the existence of a 29-qubit GHZ state with fidelity larger than 0.5. The proposed methods also succeed in the estimation of the amplitude in MLAE with the modified Grover operator where other QREM methods fail.

I. INTRODUCTION

The quantum information on quantum devices is vulnerable to various noise due to the incompleteness of the quantum state or unwanted interactions with outside world. Since the significance of quantum computing has been recognized, many quantum error correction methods was proposed for the protection of quantum information [1–4]. However, the current and near-term quantum devices are so small and noisy that those prominent methods are not yet applicable. Nevertheless, one can mitigate the errors occurring in the quantum process to obtain meaningful results on the current and near-future quantum devices. Error mitigation aims to directly retrieve the results with less noise by adding mitigation gates to the quantum circuits or performing classical post-processing after the measurements, such as zero-noise extrapolation [5–7], probabilistic error cancellation [5, 8], dynamic decoupling [9, 10], readout error mitigation for expectation value [11–14], and many new methods for various noise models [15–22]. These error mitigation techniques are often combined with the near-term quantum algorithms [23, 24].

Here we focus on the mitigation of quantum readout error, one of the significant noise factors on current near-term devices. When the state preparation noise is minimal, the readout error can be characterized by a stochastic matrix called the calibration matrix, whose elements represent the transition probability from the expected measured states to the actual measurement outputs [25, 26]. The quantum readout error mitigation

(QREM) performs classical post-processing by applying the inverse of the calibration matrix to the probability distribution (i.e., frequency distribution of measured bit-strings) obtained by the final measurement throughout the whole quantum process. Since the number of possible quantum states is 2^n for measurement of n -qubit system, rigorous inversion of calibration matrix requires exponential time and memory on classical computers. Therefore, the rigorous QREM approach to mitigate noisy probability distribution is not applicable to the measurement results from the current and near-future quantum devices with tens and hundreds of qubits.

Towards this issue, several scalable approaches have been already proposed [27, 28]. These methods assume the readout noises follow the tensor product noise model, where the readout noise on each qubit or qubit block is considered local. Under this assumption, Mooney et al. [27] sequentially apply the inverse of each small calibration matrix and cut off the vector elements smaller than the arbitrary threshold t . In their original setting, t is set to 1/10 of the shot counts, making their method quite fast, while a particular gap from the exact inversion result would occur. Although the time complexity and the space complexity of their method are not theoretically bounded, their method works enough for the witness of genuine multipartite entanglement of large GHZ states on the IBM Quantum device up to size 27 [27].

The other efficient approach by Nation et al. [28] restricts the size of the calibration matrix to the subspace of measured probability distribution and apply the inverse of the reduced calibration matrix by matrix-free iterative methods. This assumption is justified when the

measured probability distribution contains a few principal bitstrings with high probability. This method, named “mthree” (matrix-free measurement mitigation), mitigates the measurement result of a 42-qubit GHZ state from the IBM Quantum device in a few seconds on a quad-core Intel i3-10100 system with 32 GB of memory with NumPy and SciPy compiled using OpenBlas.

Our proposed methods, which were conceived independently and whose preliminary results presented in [29, 30], are similar to the idea in mthree [28]. We also assume the tensor product noise model and the reduced space of the calibration matrix. The main difference from [28] is in the order of matrix reduction and inversion.

The proposed methods directly compute each element in a reduced inverse calibration matrix while the reduction of calibration matrix comes first in [28]. This matrix inversion is the most tedious step in the proposed method, spending $O(ns^2)$ time for the measurement result with n qubits and s shots. Through experiments on real quantum devices and with numerical simulation, we show the direct computation of inverse matrix elements has advantages against the iterative method in [28].

In addition to the matrix inversion process, the mitigated frequency vector must satisfy the property of probability distributions. That is, its elements are non-negative and the element sum exactly becomes one. Since the noisy measurement results from the real devices may contain errors by various noise factor, the application of direct matrix inversion may cause negative elements in the mitigated frequency distribution. To obtain the appropriate probability distribution, the open-source software package Qiskit [31] wraps the matrix inversion process by the constrained least square optimization method and find the closest probability vector to the rigorously mitigated vector. In mthree [28], the columns of the reduced matrix are normalized again so that each of them sums to one. Once the sum of vector elements becomes one, the negative canceling method by Smolin, Gambetta, and Smith [32] (hereinafter referred to as the SGS algorithm) is applicable to find the closest probability vector in $O(N \log N)$ time for the vector size N . In the proposed methods, we first make the sum of vector elements to one after the matrix inversion process by adding a small correction vector deriving from the analytical results of the optimization problem. Here we attempt two different correction methods whose computational complexities are $O(ns)$ and $O(s)$. After the “sum-to-one” correction, the SGS algorithm is applied to the corrected frequency vector to remove the negative elements while keeping the sum of vector elements.

To check the practical performance of the proposed methods, we conduct experiments under the following three different settings whose measurement results contain all zero states or all one states with high probability, which seem to be suitable for the QREM methods. First, the difference of the expectation value of GHZ states on IBM Quantum Brooklyn (ibmq_brooklyn) device is examined among the proposed methods and the two exist-

ing methods recently proposed by Mooney et al. [27] and Nation et al. [28]. The IBM Quantum Brooklyn superconducting quantum machine provided by IBM Quantum Experience [33] is equipped with 65 qubits on Hummingbird r2 quantum processor, where the qubit connections form the heavy-hexagonal structure. The quantum volume (QV) of this device is 32. With the C++/Cython implementation, the proposed methods mitigate GHZ states up to 65 qubits within 5 seconds. We also show the proposed method outputs the standard deviation of observable arising in the mitigation process, which would be estimated smaller than actual value when using the iterative methods in [28].

Second, the fidelity of GHZ states on IBM Quantum Brooklyn is computed. The genuine multiple entanglement on the large quantum states (e.g., GHZ states and star graph states) is widely investigated by many researchers [9, 27, 34–38]. With the proposed efficient QREM, we witness the ability of QV32 IBM Quantum Brooklyn to prepare a 29-qubit GHZ state with fidelity of more than 0.5.

Furthermore, the estimation error of the maximum likelihood amplitude estimation (MLAE) algorithm [39] with modified Grover iterator [40] is investigated by numerical simulation on Qiskit [31]. The amplitude estimation problem has essential applications in finance and machine learning using quantum devices [41, 42]. The MLAE method [39, 43] avoids the phase estimation in the original amplitude estimation [44] and is expected to be realized earlier than the Shor’s algorithm as estimated in [42]. In the noiseless environment, the estimation error of this modified Grover algorithm would scale in the order of $O(1/N)$ for N Grover oracle iterations, while even a small readout noise would spoil this convergence rate. The proposed QREM methods succeed in recovering the original convergence rate of the estimation error under readout noises on the noisy simulator. In addition, while the MLAE with modified Grover iteration [40] is tolerant to depolarization errors, this numerical simulation suggests that it can also cope with readout noises.

II. PROPOSED METHODS

A. Tensor Product Noise Model

Under the complete noise model, the calibration matrix A is obtained by examining the state transition probability in the measurement process for all combinations of 2^n bitstrings of quantum states and thus sized $2^n \times 2^n$. Although the information of correlated errors among qubits due to the leakage of the measurement pulse are also included in addition to the local bit flipping on each qubit, making the complete calibration matrix is not scalable in terms of both the matrix size and the measurement cost.

Fortunately, on the near-term devices provided by IBM Quantum Experience, the correlated readout errors are

experimentally shown to be small enough that one can assume the readout error as either local or correlated among limited spatial extent [27]. Under this tensor product noise model, the $2^n \times 2^n$ sized calibration matrix A for n -qubit measurement process can be seen as a tensor product of fractions of small calibration matrices of local qubit blocks. This noise model may solve the scalability issue in the complete noise model. The number of measurements to prepare the local calibration matrices are drastically reduced from 2^n to $O(n2^k)$ and the memory to store the calibration matrices is also reduced from $O(4^n)$ to $O(n4^k)$, where k is the size of the biggest complete-calibration block.

This tensor product noise model is widely used such as in the standard QREM library of Qiskit Ignis and in other recent works [11, 27, 28]. We also develop our proposed QREM methods under this noise model. Hereinafter, for convenience, we assume the measurement error is completely local, that is,

$$A := \bigotimes_{i=0}^n A^{(i)}, \quad (1)$$

where $A^{(i)}$ is the 2×2 calibration matrix of qubit i . With the increase of computational complexity according to the size of locally complete-mitigation block, the following argument is also applicable to the general tensor product noise models with local calibration matrices for the different sizes of local complete readout channel blocks.

B. Problem Setting

We are considering the following problem for QREM. An n -qubit measurement result is given as a probability distribution $y \in \mathbb{R}^{|S|}$ where $S \subseteq \{0, 1\}^n$ is the subspace of all measured bistrings with non-zero probability. Assuming the tensor product noise model, we can also get access to the local calibration matrix $A^{(i)}$ for each qubit i . Then the task of QREM is to find a probability vector $\tilde{x}_S \in \mathbb{R}^{|S|}$ that is closest to the probability vector x satisfying $y = Ax$, where the subscript S to the vector (or matrix) x emphasize that the elements of x are in the subspace S . It is also possible to modify the problem to find the extended probability distribution with elements in the subspace S and subspace of bitstrings that are distant from S in Hamming distance d .

To efficiently solve the defined optimization problem, we will take the following three steps. For the first step, apply the reduced inverse calibration matrix $(A^{-1})_S$ to y and get roughly mitigated vector $x_S \in \mathbb{R}^{|S|}$ (Step 1). Then, find a correction vector Δ_S that adjusts the sum of elements of $x_S = (A^{-1})_S y$ into one (Step 2). Here we propose two different ways to prepare the correction vector. Finally, cancel the negative values in the corrected vector $\hat{x}_S = x_S + \Delta_S \in \mathbb{R}^{|S|}$ to output the proper probability distribution $\tilde{x}_S \in \mathbb{R}^{|S|}$ (Step 3).

C. Step 1: Matrix Inverse

Since the calibration data are given by $n \times 2$ matrices, $A^{(0)}, \dots, A^{(n-1)}$, each element of reduced inverse matrix $(A^{-1})_S$ can be computed in $O(n)$ time respectively by the following way.

$$(A^{-1})_{ij} = \prod_{k=0}^{n-1} (A^{(k)})_{i(k),j(k)}^{-1} \quad (2)$$

where $i(k)$ is the k -th digit in binary representation of index i . The algorithm for this step is described by the algorithm 1 in Appendix. This process to prepare the reduced inverse matrix requires $O(n|S|^2)$ time and $O(|S|^2)$ memory. Once we obtained $(A^{-1})_S$, the roughly mitigated vector x_S is computed by the product of $(A^{-1})_S$ and y , i.e. $x_S = (A^{-1})_S y$.

Note that it is also possible to compute x_S without explicitly preparing $(A^{-1})_S$ as below.

$$(x_S)_i = \sum_{j \in S} \prod_{k=0}^{n-1} (A^{(k)})_{i(k),j(k)}^{-1} y_j \quad (3)$$

Then it only requires half the time of making $(A^{-1})_S$ and applying it to y , and only requires $O(|S|)$ memory. In addition, since this step computes the elements of $(A^{-1})_S$ independently, it is compatible with parallel computing frameworks.

The uncertainty occurring in this step can be evaluated in the same way as mthree [28]. The mitigation overhead M is determined by the 1-norm of the reduced inverse matrix, $\mathcal{M} = \|(A^{-1})_S\|_1^2$ [11]. For an observable O , the upper bound on the standard deviation of O becomes

$$\sigma_O = \sqrt{\mathcal{M}/s} \quad (4)$$

where s is the number of samples. Unlike mthree, the mitigation overhead \mathcal{M} can be rigorously computed because the reduced inverse matrix is explicitly constructed in this step.

D. Step 2: Making the Sum of Vector Elements to One

Next is to find a correction vector Δ_S that makes the element sum of the vector to one. To compute Δ_S , we first consider the full-sized calibration matrix A and full-sized probability vector y where the empty elements are set to zero. Let \hat{x} be $\hat{x} = x + \Delta$. Then Δ is approximated based on the following least square problem.

$$\underset{\Delta}{\text{minimize}} \quad \|A\hat{x} - y\|^2 = \|A\Delta\|^2 \quad (5)$$

$$\text{subject to} \quad 1^T \cdot \hat{x} = 1 \quad (6)$$

1. Approach 1 (delta)

In the first approach, we perform the singular value decomposition (SVD) of A and convert the optimization problem above to the form which is analytically solvable. Let the SVD of A be $A = U\Sigma V^T = \sum_{i=0}^{N-1} \sigma_i u_i v_i^T$ and represent Δ as $\Delta = \Delta_{j_0} v_{j_0} + \Delta_{j_1} v_{j_1} + \dots + \Delta_{j_{k-1}} v_{j_{k-1}}$ using k right singular vectors $\{v_i\}$ of A . Then the problem (5) becomes

$$\begin{aligned} \min_{\Delta \in \mathbb{R}^N} \quad & \sum_{i=j_0}^{j_{k-1}} \sigma_i^2 \Delta_i^2 \\ \text{subject to} \quad & \sum_{i=j_0}^{j_{k-1}} (1^T \cdot v_i) \Delta_i = 1 - 1^T \cdot x. \end{aligned} \quad (7)$$

This constrained least square problem can be rigorously solved by Lagrange multiplier. Each coefficient of $\Delta = \Delta_{j_0} v_{j_0} + \Delta_{j_1} v_{j_1} + \dots + \Delta_{j_{k-1}} v_{j_{k-1}}$ can be computed as

$$\Delta_i = \frac{1 - 1^T \cdot x}{\sum_{l=j_0}^{j_{k-1}} \frac{(1^T \cdot v_l)^2}{\sigma_l^2}} \cdot \frac{1^T \cdot v_i}{\sigma_i^2}. \quad (8)$$

Since the calibration matrix A is the tensor product of small matrix $A^{(i)}$ for each qubit i , the values $\sigma_i, 1^T \cdot v_i$ can be computed in $O(n)$ time using the property of $(U_1 \Sigma_1 V_1^T) \otimes (U_2 \Sigma_2 V_2^T) = (U_1 \otimes U_2)(\Sigma_1 \otimes \Sigma_2)(V_1^T \otimes V_2^T)$ for the SVD of two matrices $A_1 = U_1 \Sigma_1 V_1^T$ and $A_2 = U_2 \Sigma_2 V_2^T$. Restricting the space of the vector into S , the correction vector is approximated as Δ_S . The time complexity to compute the coefficients Δ_i is $O(n|S|k)$ with arbitrary parameter k .

Furthermore, the gap of readout error probabilities $p(1|0)$ getting state 1 expected 0 and $p(0|1)$ for the vice versa, are getting smaller in current devices. When assuming $p(1|0) \simeq p(0|1)$, the coefficients of Δ can be approximated more efficiently. Now the calibration matrix of each qubit A_i becomes closer to symmetric matrix which can be eigendecomposed by Hadamard matrices. Using the property of column sum of Hadamard matrix, $1^T \cdot v_0 \gg 1^T \cdot v_i$ for $i = 1, 2, \dots$. Then Δ_i can be computed as

$$\Delta'_i = \frac{1 - 1^T \cdot x}{\frac{(1^T \cdot v_0)^2}{\sigma_0^2}} \cdot \frac{1^T \cdot v_i}{\sigma_i^2}. \quad (9)$$

In addition, (9) implies $\Delta'_0 \gg \Delta'_i$ for $i = 1, 2, \dots$. Therefore, we used $\Delta'_S = \Delta'_0 v_{0S}$ as a correction vector in numerical simulation. This step takes $O(n|S|)$ time.

2. Approach 2 (least norm)

In the second approach, we find the nearest vector to x_S by solving the following least norm problem.

$$\begin{aligned} \min_{\hat{x}_S} \quad & \|\hat{x}_S - x_S\|^2 \\ \text{subject to} \quad & \mathbf{1}^T \cdot \hat{x}_S = 1 \end{aligned} \quad (10)$$

By changing the variable with $z := \hat{x}_S - x_S$, this optimization problem above can be solved by well-known constrained least norm problem

$$\begin{aligned} \min_{\hat{x}_S} \quad & \|z\|^2 \\ \text{subject to} \quad & \mathbf{1}^T \cdot z = 1 - \mathbf{1}^T \cdot \hat{x}_S. \end{aligned} \quad (11)$$

The analytical solution of this problem is $z = \left(\frac{1 - \mathbf{1}^T \cdot x_S}{|S|} \right) \mathbf{1}$. Therefore the correction process of the second approach becomes

$$\hat{x}_S = x_S + \left(\frac{1 - \mathbf{1}^T \cdot x_S}{|S|} \right) \mathbf{1}. \quad (12)$$

This simple process only requires $O(|S|)$ time in the computation of $\mathbf{1}^T \cdot x_S$ and addition of correction term to x_S .

E. Step 3: Negative Cancelling

Finally, we are going to find the closest positive vector to \hat{x}_S which still satisfy the sum-to-one condition. In this step, the negative cancelling algorithm by Smolin, Gambetta, and Smith [32] (the SGS algorithm) is applied. Given an input vector whose element sum equals 1 but may contain negative values, this algorithm deletes the negative values and the small positive values, and also shift the positive values to lower ones based on the bounded-minimization approach using the Lagrange multiplier. The procedure of SGS algorithm is described at Algorithm 2. Through this algorithm, the finally mitigated probability vector $\tilde{x}_S = \text{sgs_algorithm}(\hat{x}_S)$ is computed in $O(|S| \log |S|)$ time. Note that the use of SGS algorithm after the main process of matrix inversion process is also mentioned at [27, 28].

III. DEMONSTRATIONS

The proposed method is implemented with C++/Eigen, and Cython, and makes use of Qiskit for calibration circuit construction and execution. The source code of the proposed methods is open to the public named “libs_qrem” [45]. For the fair comparison of the performance with existing QREM approaches, both the QREM methods of rigorous inversion of tensor calibration matrix and the method by Mooney et al. [27] are also implemented there. Since the source code of the QREM method by Nation et al. [28] is available online named “mthree” [46], we use their own implementation for comparison. Since the mthree package finally returns probability vectors with negative elements after the matrix inversion, we applied the SGS algorithm [32] to the outputs. All timing data is taken on 2.5GHz quad-core Intel Core i7 processor (Turbo Boost up to 3.7GHz) with 6MB shared L3 cache with 16GB of 1600MHz DDR3L onboard memory [47].

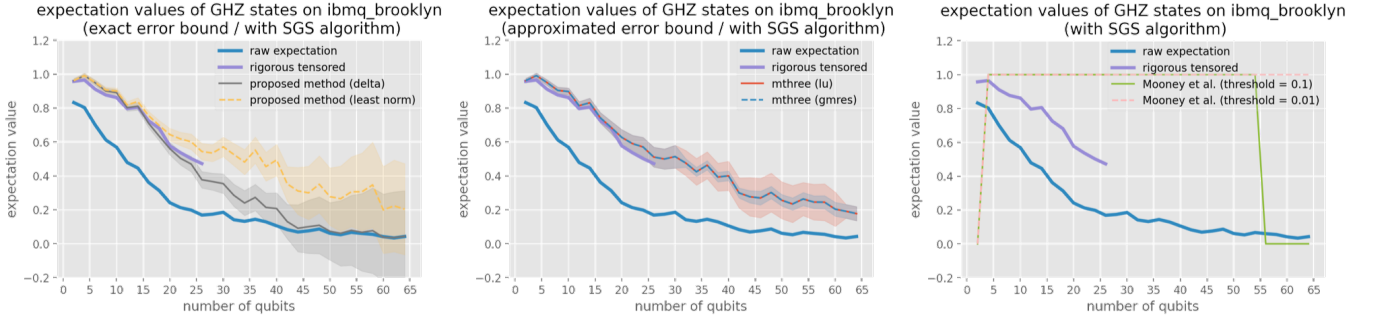


FIG. 1. The plots of expectation values against number of qubits. In the left figure, the solid (grey) line and dashed (yellow) line represent the expectation values by the proposed “delta” and “least norm” method introduced in Section II. In the middle figure, the solid (red) line and dotted (blue) line represent the expectation values mitigated by mthree package with “direct” method using LU decomposition and “iterative” method using GMRES. In the right figure, the solid (green) line and dashed (pink) line represent the mitigated expectation values by Mooney et al. with threshold $t = 0.1$ and $t = 0.01$. For reference, all figures contain the expectations with rigorous error mitigation and without error mitigation (raw expectation). The shaded areas represent error bounds evaluated by the mitigation overhead (4). All results are normalized to keep the sum of probability vector to one, as in (13).

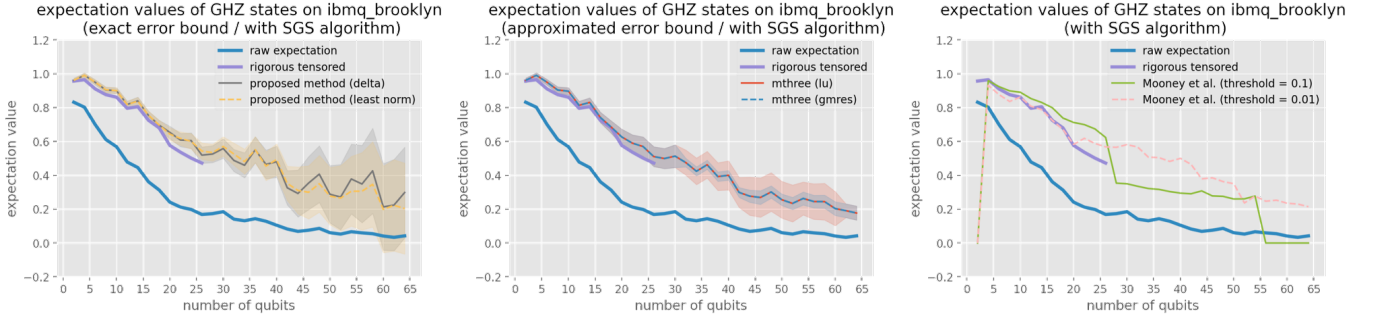


FIG. 2. The plots of expectation values against number of qubits with the normalization method (14) instead of (13). The color notations of plots are the same as those of Fig. 1.

We conducted two experiments on the 65-qubit IBM Quantum Brooklyn system: the expectation values of GHZ states and the fidelity of GHZ states. The average assignment and CNOT error rates across the qubits on IBM Quantum Brooklyn are 2.89% and 2.57% respectively. The detailed noise information and the mapping of logical qubits to physical qubits are show at Fig. 7 in Appendix B. We also conducted the numerical simulation of the modified Grover algorithm on the noisy Qiskit simulator with readout noise to investigate the precision of estimation error with different QREM methods.

A. Expectation Value of GHZ States on IBM Quantum Brooklyn

First, the mitigated expectation values of GHZ states on IBM Quantum Brooklyn are examined, which is also used as the benchmarking for QREM in [28]. The expectation value of the observable O is computed by the following way. Given a raw or mitigated frequency distribution p as a dictionary of bitstrings to their probabil-

ities, the expectation $\langle O \rangle$ is computed by

$$\langle O \rangle = \frac{1}{\text{sum}(p)} \sum_i O(i)p_i \quad (13)$$

where $\text{sum}(p)$ is the sum of elements in p , $O(i)$ is the value of observable O for state i , and p_i is the element in p for the number of shots for state i . Here the expectation value is divided by the sum of elements in p because the mitigated vector might not satisfy the condition of $\text{sum}(p) = 1$.

We took the expectation value with the observable $O = \sigma_Z^{(0)} \otimes \dots \otimes \sigma_Z^{(n-1)}$, measuring all the qubits in computational bases. The expectations of GHZ state with the even number of qubits are supposed to be 1 under the noiseless environment.

Figures in Fig. 1 show the actual expectation value of GHZ states on IBM Quantum Brooklyn with and without the QREMs. The mitigation of rigorous inversion of calibration matrix method was performed up to 26-qubit states. Other efficient QREM methods are performed totally up to 65-qubit measurement results. The shaded regions give the error bounds by mitigation process which

is computed by the mitigation overhead and the number of samples [11].

The left figure in Fig.1 extracts the plots of two proposed methods (“delta”, “least norm”) and the rigorously mitigated expectation values after applying the SGS algorithm. Expectations by the least norm method are clearly higher than the rigorous inversion of tensor calibration matrix, while the expectations by delta method are closer to the plots of rigorous inversion. Note that the 1-norm of the reduced inverse matrix $(A^{-1})_S$ used in the computation of error bounds is directly and exactly computed by the equation ((4)).

On the other hand, the central figure in Fig. 1 shows the plots of expectation values with QREM by the mthree packages. Their expectation values are also higher than the rigorously mitigated ones to the same extent as the plots by the proposed “least norm” method. Since the inversion of $(A_S)^{-1}$ requires $O(|S|^3)$ times, one can only get access to the approximated error bound through the mthree package for large quantum states. In addition, the estimated error bound may not always correspond to the exact error bound. The error bounds through exact computation of $\|(A_S)^{-1}\|_1$ and the error bounds in the mthree package through the iteratively approximated $\|(A_S)^{-1}\|_1$ by Higham’s implementation [48] of Hager’s method [49] are shown in Fig. 3.

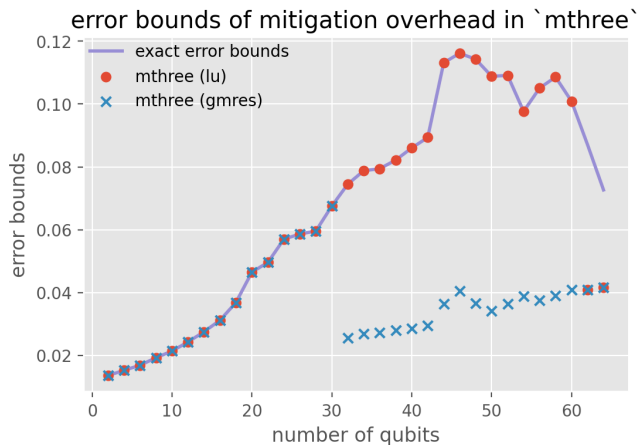


FIG. 3. The upper bound on the standard deviation for the expectation of GHZ states with the even number of qubits. The label “exact error bounds” denotes the error bounds directly computed from equation (4). The label “mthree (lu)” denotes the error bounds computed by Hager’s algorithm using LU decomposition in the mthree package. The label “mthree (gmres)” denotes the error bounds computed by Hager’s algorithm with GMRES iterative method in the mthree package.

We can also see from the right side figure of Fig. 1 that the QREM method of Mooney et al. returns the expectation value 1 for almost all the size of GHZ state. Since the mitigated frequency distributions by this method may not take the element sum to one, the expectation values are normalized by (13) as explained above. On the other

hand, we can consider another way to compute expectation value as (14).

$$\langle O \rangle = \sum_i O(i)p_i, \quad (14)$$

Here we assume the sum of elements of the mitigated frequency distribution is 1, although it may vary through the mitigation process. This type of expectation values can be seen as the direct counts of the frequency of the bitstrings in the mitigated vector.

The expectation values using this calculation method are shown in Fig. 2. In the right figure of Fig. 2, the mitigated expectation values by Mooney et al.’s method, especially with the threshold 0.01, are close to the rigorously mitigated values. This can be interpreted as counting the all-zero state and all-one state $|00\dots 0\rangle, |11\dots 1\rangle$ in the mitigated vector. By using the equation (14), the expectation values of proposed “delta” method become higher as shown in the left figure of Fig. 2, because the elements of probability distributions by “delta” method in larger system sizes would no longer sum up to exactly 1. The gap from 1 becomes even larger for the measurement results of large system while we still use reduced calibration matrix in the small subspace. Since the “least norm” method strictly adjust the element sum of the vector to one and mthree uses the quasi-probability in the reduced matrix, the expectation values by these QREM methods take the same values as those in Fig. 1.

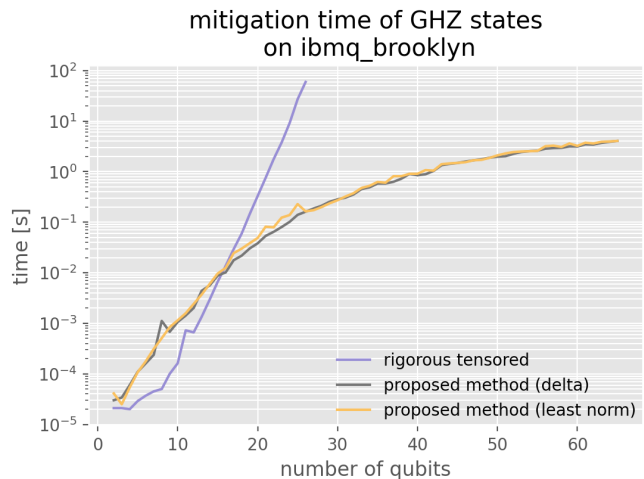


FIG. 4. The plots of mitigation time by proposed methods and rigorous inversion of tensor calibration matrix. The mitigation time (y-axis) is shown with log-scale. The purple line denotes the mitigation time by rigorous inversion of tensor calibration matrices. The black line denotes the mitigation time by the proposed “delta” QREM method, and the black line denotes the mitigation time by the proposed “least norm” QREM method.

In addition, the mitigation time of the proposed QREM method is plotted in Fig. 4. We can see the rigorous mitigation by the tensor product noise model requires exponential time resources. Fig. 4 implies both of

the proposed methods mitigate the 65-qubit GHZ states in 5 seconds on the 2015 model MacBook pro [47], which is practically fast enough for the mitigation of measurement results from large quantum devices. This high-speed post-processing also owes to the C++/Cython implementation.

B. Fidelity of GHZ States on IBM Quantum Brooklyn

Next, the fidelity of GHZ states on IBM Quantum Brooklyn was investigated. We computed the fidelity by multiple quantum coherence (MQC), following the procedure in the experiments by Wei et al.'s [9] and Mooney et al. [27]. The GHZ fidelity F can be calculated as

$$F := \frac{P + C}{2} \quad (15)$$

where the population $P = \langle 0 \dots 0 | \rho | 0 \dots 0 \rangle + \langle 1 \dots 1 | \rho | 1 \dots 1 \rangle$ can be directly measured as the GHZ populations and the coherence $C = |\langle 1 \dots 1 | \rho | 0 \dots 0 \rangle| + |\langle 0 \dots 0 | \rho | 1 \dots 1 \rangle|$ can be measured through the multiple quantum coherences (MQC) [9, 50, 51]. Here the coherence C is indirectly computed by the following overlap signals $S_\phi = \text{Tr}(\rho_\phi \rho)$, where $\rho_\phi = e^{-i\frac{\phi}{2} \sum_j \sigma_z^j} \rho e^{i\frac{\phi}{2} \sum_j \sigma_z^j}$ is prepared by applying the rotation-Z gates on each qubits. Using S_ϕ with different angle ϕ , the coherence is calculated as $C = 2\sqrt{I_N}$ with

$$I_q = \mathcal{N}^{-1} \left| \sum_{\phi} e^{iq\phi} S_\phi \right| \quad (16)$$

where \mathcal{N} is the number of angles ϕ .

The fidelity is averaged over 8 independent runs with 8192 shots as Wei et al. [9] and Mooney et al. [27] performed. Here the fidelity greater than 0.5 is sufficient to confirm the good multipartite entanglement on the real device.

The fidelity of GHZ states was examined up to size 39 on 65-qubit IBM Quantum Brooklyn device. The different QREM methods are applied to the raw probability distributions. The QREM with rigorous inversion of tensor calibration matrices are performed up to 30 qubits, while other QREM methods are performed up to 39-qubits.

The results are shown in the Fig. 5. The raw results without QREM score the fidelity over 0.5 up to 17 qubit size, while the results with QREM by the proposed method with least square method record the higher fidelities that exceed 0.5 up to qubit size 29 (see Table I). Note that the fidelity values estimated by the proposed QREM with the least norm problem method closely follow the plots of rigorously mitigated fidelities, while the fidelity plots by other QREM methods have more gaps from the rigorously mitigated fidelities. The fidelities by the proposed method are also smaller than the fidelities by Mooney et al.'s method. From the mitigation results

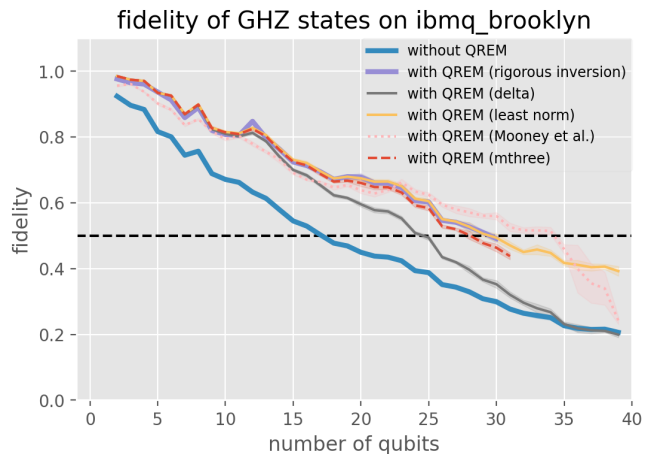


FIG. 5. The fidelities of GHZ states on IBM Quantum Brooklyn estimated by different QREM methods. The blue line shows the raw fidelities without QREM. The purple line shows the rigorously mitigated fidelities under the tensor product noise model. The black, yellow, pink, and red lines respectively shows the fidelities mitigated by the proposed QREM with delta method, by the proposed QREM with least norm problem method, by the Mooney et al.'s method with threshold 0.01, and by the mthree package with the direct LU decomposition method.

by Mooney et al.'s method we can observe the 34-qubit GHZ states also scored the fidelity over 0.5 (see Fig. 5).

Compared to expectation values of the GHZ state, the QREM on the fidelities of the GHZ state seems more effective. The computation of fidelity only uses the populations of all-zero bitstring and all-one bitstring in the probability distribution, while the computation of expectation value adds up the populations of all the measured bitstrings. Since the GHZ state only outputs the all-zero and all-one states under the noiseless environment, other bitstrings can be considered as the by-product of various error factors. However, as the size of the quantum state gets larger, the state preparation error becomes significantly large, which generates more unwanted bitstrings in the result probability distribution that would make the computation of expectation value more inaccurate. Therefore, we can see the readout error mitigation methods for noisy probability distributions are more suitable for recovering the dominant populations in the original probability distribution.

C. Maximum Likelihood Amplitude Estimation with Modified Grover Iterator

Finally, we conduct a Monte Carlo integration by maximum likelihood amplitude estimation (MLAE) algorithm with modified Grover iterator proposed by Uno et al., which is also called modified Grover algorithm [40]. This experiment is also aimed to investigate the existence of applications of the proposed method to prospective quan-

TABLE I. The comparison of measured and mitigated fidelity of GHZ states from 27-qubit to 31-qubit among the rigorous matrix inversion, the proposed “delta” method, the proposed “least norm” method, Mooney et al.’s method with threshold 0.01, and the mthree package with “direct” method using LU decomposition.

size	raw	rigorous inversion	proposed (delta)	proposed (least norm)	Mooney et al. ($t = 0.01$)	mthree (lu)
27	0.344 ± 0.004	0.541 ± 0.005	0.420 ± 0.005	0.543 ± 0.004	0.580 ± 0.012	0.520 ± 0.004
28	0.330 ± 0.007	0.527 ± 0.013	0.397 ± 0.010	0.527 ± 0.013	0.571 ± 0.012	0.502 ± 0.012
29	0.308 ± 0.004	0.510 ± 0.008	0.367 ± 0.006	0.506 ± 0.008	0.561 ± 0.007	0.478 ± 0.007
30	0.299 ± 0.008	0.491 ± 0.012	0.353 ± 0.012	0.494 ± 0.012	0.560 ± 0.011	0.464 ± 0.012
31	0.277 ± 0.006	-	0.321 ± 0.009	0.471 ± 0.011	0.526 ± 0.013	0.438 ± 0.010

TABLE II. The parameters used in the numerical simulation. We tried all different condition among the number of qubits, shots for Grover circuits, and the rate readout noise. The variable m represents the number of Grover iteration in each quantum circuit used in the MLAE algorithm, which is the same among the different conditions.

parameter	parameter name	examined values
number of qubits	n	{10, 20}
shots for Grover circuits	N_{shot}	{100, 8192}
shots for calibration circuits	-	{8192}
number of Grover iteration	m	[1, 2, 4, 8, 16, 32, 64]
target values	$I = \sin^2 \theta$	$b_{max} = \{1/2\}$
readout noise	$p(0 1) = p(1 0)$	{0.01, 0.03, 0.05}

tum algorithms. The whole procedure to estimate the amplitude follows the original MLAE algorithm [39], running quantum circuits of shallower Grover iterator with different iterations. The MLAE algorithm has two big advantages against the original amplitude estimation algorithm using quantum Fourier transformation (QFT) [44], one is avoiding the QFT to make the circuit shallower and the other is using less controlled gates.

The modified Grover algorithm only differs from the MLAE algorithm in the construction of Grover iterator, which is represented as $Q = U_0 A^\dagger U_f A$, where U_0 and U_f are the reflection operators defined as

$$\begin{aligned} U_0 &= -\mathbf{I}_{n+1} + 2|0\rangle_{n+1}\langle 0|_{n+1}, \\ U_f &= -\mathbf{I}_{n+1} + 2\mathbf{I}_n \otimes |0\rangle\langle 0|. \end{aligned} \quad (17)$$

The $(n+1)$ -qubit initial state $|0\rangle_{n+1}$ after m iterations of operator Q becomes

$$Q^m |0\rangle_{n+1} = \cos(2m\theta) |0\rangle_{n+1} + \sin(2m\theta) |\phi\rangle_{n+1} \quad (18)$$

where $|\phi\rangle_{n+1}$ is an unknown state orthogonal to $|0\rangle_{n+1}$. Then, the probability of getting state $|0\rangle_{n+1}$ with the angle θ and the number of iteration m is represented as $p_Q(0; \theta, m) = \cos^2(2m\theta)$. Hence it is enough to know the probability of getting state $|0\rangle_{n+1}$ in (18) to estimate the target value θ . This type of probability distribution seems to be compatible with applying the proposed QREM algorithm since it is expected to get $|0\rangle_{n+1}$ state with high frequency.

According to the MLAE algorithm [39], following the Heisenberg limit, the lower bound of the estimation error of θ decreases at most in the speed of $O(1/\sqrt{N_q})$ for $N_q = \sum_i m_i$ queries. In contrast, the estimation error converges in the order of $O(1/N_q)$ for N_q rounds of Grover iterations, which achieves the quadratic speedup. The performance of the modified Grover algorithm can be

checked by the decrease in the rate of estimation errors and how well the estimation errors follow the order of $O(1/N_q)$, which is referred to as the Heisenberg limit.

Next, let us briefly review the numerical integration by Grover search following the procedures in [39]. Using the notations of [39], we focus on the following integration:

$$\begin{aligned} I &= \frac{1}{b_{max}} \int_0^{b_{max}} \sin(x)^2 dx \\ &= \frac{1}{b_{max}} \left(\frac{b_{max}}{2} - \frac{1}{4} \sin(2b_{max}) \right), \end{aligned} \quad (19)$$

where b_{max} is a constant parameter. The target value I can be discretized as

$$S = \sum_{x=0}^{2^n-1} p(x) \sin^2 \left(\frac{(x + \frac{1}{2}) b_{max}}{2^n} \right), \quad (20)$$

which can be estimated via the amplitude estimation algorithm and thus the modified Grover algorithm is applicable.

We run the numerical simulation of this modified Grover algorithm on the Qiskit simulator. The simulation was performed with 10-qubit and 20-qubit search space, respectively, on the Qiskit simulator [31]. The parameter of the modified Grover algorithm following the notation in [40] is shown in Table II. Since the current QV32 IBM Quantum devices has average readout assignment error from 0.02 to 0.03, we tested different readout error rates with $p(0|1) = p(1|0) = \{0.01, 0.03, 0.05\}$.

The results of the numerical simulation are shown in Fig. 6, 8, 9, and 10. Since the estimation error properties of different settings between 10-qubit and 20-qubit systems and between 100 shots and 8192 shots are quite similar, we only show the plots of 10-qubit system with

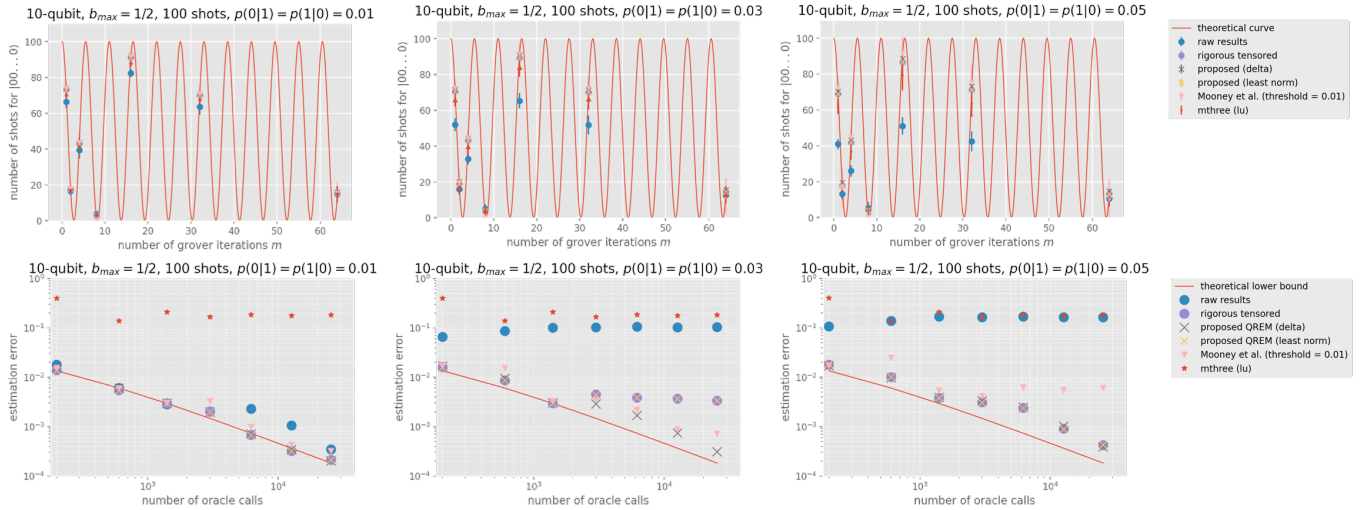


FIG. 6. The number of shots measuring $|0\rangle_{n+1}$ state and the estimation error of Monte Carlo integration on the 10-qubit system where the circuit of Grover iterators are sampled with 100 shots. The figures in the upper row show the shot count of $|0\rangle_{n+1}$ state. The red sine waves represent the shot count of $|0\rangle_{n+1}$ state under the ideal condition without noise. The other plots represent the measured shot counts by different QREM methods with error bars. The figures in the lower row show the estimation error of Monte Carlo integration. The red lines represent the theoretical lower bound of estimation error (Heisenberg limit). The other plots represent the estimation errors by different QREM methods.

100 shots as Fig. 6. Other figures can be found at Appendix C. In these figures, the upper rows show the numbers of shots getting $|0\rangle_{n+1}$ and the lower rows show the estimation errors. All the plots are averaged over ten independent trials. Plots of each color show the theoretical values (red curves), the raw results (blue, “o”), the rigorously mitigated results (purple, “o”), the mitigated results by proposed QREM with delta method (black, “x”), the mitigated results by proposed QREM with least norm method (yellow, “x”), the mitigated results by Mooney et al.’s method with threshold $t = 0.01$ (pink, “v”), and the mitigated results by mthree’s direct method using the mthree package (red “*”). Since the plots of Mooney et al.’s method with threshold $t = 0.1$ are so close to those of Mooney et al.’s method with threshold $t = 0.01$, they are not shown in the figures. Likewise, the plots of mthree’s iterative method are also omitted because they are so close to the plots of mthree’s direct method.

Again, we only focus on the results of 10-qubit system with 100-shots in Fig. 6. In Fig. 6, estimation without QREM fails when the readout errors are set to 0.03 and 0.05, while the estimation errors by the rigorous mitigation and by the proposed methods successfully decrease, following the Heisenberg limit. Compared with Mooney et al.’s method, the proposed methods exhibit better estimation accuracy, and both the shot counts of $|0\rangle_{n+1}$ and the estimation error are closer to the rigorously mitigated plots, which is more obvious with 8192 shots (see Fig. 8 in Appendix C). On the other hand, the plots by mthree library fail to estimate the target angle θ for all the experiment settings. Since the shot counts of $|0\rangle_{n+1}$ mitigated by mthree library are also close to the rigorously mitigated ones, we can see the subtle difference in

the mitigation results may greatly affect the subsequent process, and thus the mitigation accuracy is significant in the QREM process.

Through these results, it can be said that the modified Grover algorithm is more compatible with the proposed QREM methods to mitigate the readout error. Besides, while the modified Grover algorithm [40] is tolerant to the depolarizing error, these simulation results also support the ability of the modified Grover algorithm to overcome the readout noise even in the large system over 100-qubit.

IV. CONCLUSION

The proposed QREM methods mitigate the readout error in $O(ns^2)$ time and $O(s)$ memory with n qubits and s shots through the post-processing on classical computers. This means the proposed methods scale linearly to the number of finally measured qubits for fixed shot counts, which provides a scalable QREM tool for the current and near-future quantum devices with larger qubits.

Experiments of GHZ states on IBM Quantum Brooklyn and numerical experiments of modified Grover algorithm support the advantage of the proposed QREM methods. The proposed QREM methods mitigate the expectation values of 65-qubit GHZ states on IBM Quantum Brooklyn with exact mitigation overhead while other existing QREM methods can only output the approximated mitigation overhead due to the increase of the computational complexity. Using the proposed QREM methods, we also witnessed the 29-qubit multipartite entanglement of GHZ state on IBM Quantum Brooklyn

with fidelity 0.506 ± 0.008 .

The numerical simulation on the modified Grover algorithm also supports the advantage of the proposed QREM methods. The estimation errors of target value θ under different readout noise levels on the 10-qubit system and 20-qubit system are investigated. In these settings, the proposed methods record the best accuracy among the recently proposed efficient QREM methods. Therefore, we can find effective applications of the proposed QREM method on such significant quantum algorithms that would be realizable in the near future. In addition, it can be conversely said that the proposed QREM methods provide a solution to run the modified Grover

algorithm under readout noise, revealing the additional advantage of the modified Grover algorithm which is already tolerant to the depolarizing noise.

ACKNOWLEDGMENTS

We thank Prof. Hiroshi Imai at the Graduate School of Information Science and Technology, The University of Tokyo, for the insightful, related discussions and comments. The results presented in this paper were obtained in part using an IBM Quantum computing system as part of the IBM Quantum Hub at The University of Tokyo.

-
- [1] P. W. Shor, Phys. Rev. A **52**, R2493 (1995).
 [2] A. M. Steane, Phys. Rev. Lett. **77**, 793 (1996).
 [3] A. Kitaev, Annals of Physics **303**, 2–30 (2003).
 [4] C. Chamberland, G. Zhu, T. J. Yoder, J. B. Hertzberg, and A. W. Cross, Phys. Rev. X **10**, 011022 (2020).
 [5] K. Temme, S. Bravyi, and J. M. Gambetta, Phys. Rev. Lett. **119**, 180509 (2017).
 [6] A. Kandala, K. Temme, A. D. Córcoles, A. Mezzacapo, J. M. Chow, and J. M. Gambetta, Nature **567**, 491 (2019).
 [7] T. Giurgica-Tiron, Y. Hindy, R. LaRose, A. Mari, and W. J. Zeng, 2020 IEEE International Conference on Quantum Computing and Engineering (QCE) (2020).
 [8] R. Takagi, Physical Review Research **3**, 033178 (2021).
 [9] K. X. Wei, I. Lauer, S. Srinivasan, N. Sundaresan, D. T. McClure, D. Toyli, D. C. McKay, J. M. Gambetta, and S. Sheldon, Phys. Rev. A **101**, 032343 (2020).
 [10] B. Pokharel, N. Anand, B. Fortman, and D. A. Lidar, Phys. Rev. Lett. **121**, 220502 (2018).
 [11] S. Bravyi, S. Sheldon, A. Kandala, D. C. McKay, and J. M. Gambetta, Phys. Rev. A **103**, 042605 (2021).
 [12] E. van den Berg, Z. K. Mineev, and K. Temme, Model-free readout-error mitigation for quantum expectation values (2021), arXiv:2012.09738 [quant-ph].
 [13] S. Chen, W. Yu, P. Zeng, and S. T. Flammia, PRX Quantum **2**, 030348 (2021).
 [14] R. Hicks, C. W. Bauer, and B. Nachman, Phys. Rev. A **103**, 022407 (2021).
 [15] J. R. McClean, Z. Jiang, N. C. Rubin, R. Babbush, and H. Neven, Nature Communications **11** (2020).
 [16] N. Yoshioka, H. Hakoshima, Y. Matsuzaki, Y. Tokunaga, Y. Suzuki, and S. Endo, Generalized quantum subspace expansion (2021), arXiv:2107.02611 [quant-ph].
 [17] S. Endo, Z. Cai, S. C. Benjamin, and X. Yuan, Journal of the Physical Society of Japan **90**, 032001 (2021).
 [18] S. Endo, Q. Zhao, Y. Li, S. Benjamin, and X. Yuan, Phys. Rev. A **99**, 012334 (2019).
 [19] P. Czarnik, A. Arrasmith, P. J. Coles, and L. Cincio, Quantum **5**, 592 (2021).
 [20] A. Strikis, D. Qin, Y. Chen, S. C. Benjamin, and Y. Li, PRX Quantum **2**, 040330 (2021).
 [21] J. Sun, X. Yuan, T. Tsunoda, V. Vedral, S. C. Benjamin, and S. Endo, Phys. Rev. Applied **15**, 034026 (2021).
 [22] M. Otten and S. K. Gray, npj Quantum Information **5**, 11 (2019).
 [23] A. Peruzzo, J. McClean, P. Shadbolt, M.-H. Yung, X.-Q. Zhou, P. J. Love, A. Aspuru-Guzik, and J. L. O’Brien, Nature Communications **5** (2014).
 [24] E. Farhi, J. Goldstone, and S. Gutmann, A quantum approximate optimization algorithm (2014), arXiv:1411.4028 [quant-ph].
 [25] J. S. Lundeen, A. Feito, H. Coldenstrodt-Ronge, K. L. Pregnell, C. Silberhorn, T. C. Ralph, J. Eisert, M. B. Plenio, and I. A. Walmsley, Nature Physics **5**, 27 (2009).
 [26] F. B. Maciejewski, Z. Zimborás, and M. Ozmaniec, Quantum **4**, 257 (2020).
 [27] G. J. Mooney, G. A. L. White, C. D. Hill, and L. C. L. Hollenberg, Journal of Physics Communications **5**, 095004 (2021).
 [28] P. D. Nation, H. Kang, N. Sundaresan, and J. M. Gambetta, PRX Quantum **2**, 040326 (2021).
 [29] B. Yang and R. Raymond, in *SIG on Quantum Software, Information Processing Society of Japan* (2021) <https://www.ipsj.or.jp/kenkyukai/event/qs3.html>.
 [30] B. Yang, R. Raymond, and S. Uno, in *Asian Quantum Information Science Conference* (2021) <https://drive.google.com/file/d/1FWdra51hpyACE0gIOcka1FQRxAftso5N/view?usp=sharing>.
 [31] G. Aleksandrowicz, T. Alexander, P. Barkoutsos, L. Bello, Y. Ben-Haim, D. Bucher, F. J. Cabrera-Hernández, J. Carballo-Franquis, A. Chen, C.-F. Chen, J. M. Chow, A. D. Córcoles-Gonzales, A. J. Cross, A. Cross, J. Cruz-Benito, C. Culver, S. D. L. P. González, E. D. L. Torre, D. Ding, E. Dumitrescu, I. Duran, P. Eendebak, M. Everitt, I. F. Sertage, A. Frisch, A. Fuhrer, J. Gambetta, B. G. Gago, J. Gomez-Mosquera, D. Greenberg, I. Hamamura, V. Havlicek, J. Hellmers, Lukasz Herok, H. Horii, S. Hu, T. Imamichi, T. Itoko, A. Javadi-Abhari, N. Kanazawa, A. Karazeev, K. Krsulich, P. Liu, Y. Luh, Y. Maeng, M. Marques, F. J. Martín-Fernández, D. T. McClure, D. McKay, S. Meesala, A. Mezzacapo, N. Moll, D. M. Rodríguez, G. Nannicini, P. Nation, P. Ollitrault, L. J. O’Riordan, H. Paik, J. Pérez, A. Phan, M. Pistoia, V. Prutyaynov, M. Reuter, J. Rice, A. R. Davila, R. H. P. Rudy, M. Ryu, N. Sathaye, C. Schnabel, E. Schoute, K. Setia, Y. Shi, A. Silva, Y. Siraichi, S. Sivarajah, J. A. Smolin, M. Soeken, H. Takahashi, I. Tavernelli, C. Taylor, P. Taylour, K. Trabing, M. Treinish, W. Turner, D. Vogt-Lee, C. Vuillot, J. A. Wildstrom,

- J. Wilson, E. Winston, C. Wood, S. Wood, S. Wörner, I. Y. Akhalwaya, and C. Zoufal, Qiskit: An Open-source Framework for Quantum Computing (2019).
- [32] J. A. Smolin, J. M. Gambetta, and G. Smith, *Phys. Rev. Lett.* **108**, 070502 (2012).
- [33] IBM Quantum Experience (2016).
- [34] C. Song, K. Xu, W. Liu, C.-p. Yang, S.-B. Zheng, H. Deng, Q. Xie, K. Huang, Q. Guo, L. Zhang, P. Zhang, D. Xu, D. Zheng, X. Zhu, H. Wang, Y.-A. Chen, C.-Y. Lu, S. Han, and J.-W. Pan, *Phys. Rev. Lett.* **119**, 180511 (2017).
- [35] M. Gong, M.-C. Chen, Y. Zheng, S. Wang, C. Zha, H. Deng, Z. Yan, H. Rong, Y. Wu, S. Li, F. Chen, Y. Zhao, F. Liang, J. Lin, Y. Xu, C. Guo, L. Sun, A. D. Castellano, H. Wang, C. Peng, C.-Y. Lu, X. Zhu, and J.-W. Pan, *Phys. Rev. Lett.* **122**, 110501 (2019).
- [36] C. Song, K. Xu, H. Li, Y.-R. Zhang, X. Zhang, W. Liu, Q. Guo, Z. Wang, W. Ren, J. Hao, H. Feng, H. Fan, D. Zheng, D.-W. Wang, H. Wang, and S.-Y. Zhu, *Science* **365**, 574 (2019), <https://www.science.org/doi/pdf/10.1126/science.aay0600>.
- [37] G. J. Mooney, C. D. Hill, and L. C. L. Hollenberg, *Scientific Reports* **9** (2019).
- [38] B. Yang, R. Raymond, H. Imai, H. Chang, and H. Hiraishi, Testing scalable bell inequalities for quantum graph states on ibm quantum devices (2021), [arXiv:2101.10307](https://arxiv.org/abs/2101.10307) [quant-ph].
- [39] Y. Suzuki, S. Uno, R. Raymond, T. Tanaka, T. Onodera, and N. Yamamoto, *Quantum Information Processing* **19** (2020).
- [40] S. Uno, Y. Suzuki, K. Hisanaga, R. Raymond, T. Tanaka, T. Onodera, and N. Yamamoto, *New Journal of Physics* **23**, 083031 (2021).
- [41] T. Giurgica-Tiron, I. Kerenidis, F. Labib, A. Prakash, and W. Zeng, Low depth algorithms for quantum amplitude estimation (2020), [arXiv:2012.03348](https://arxiv.org/abs/2012.03348) [quant-ph].
- [42] A. Bouland, W. van Dam, H. Joorati, I. Kerenidis, and A. Prakash, Prospects and challenges of quantum finance (2020), [arXiv:2011.06492](https://arxiv.org/abs/2011.06492) [q-fin.CP].
- [43] T. Tanaka, Y. Suzuki, S. Uno, R. Raymond, T. Onodera, and N. Yamamoto, *Quantum Information Processing* **20**, 293 (2021).
- [44] G. Brassard, P. Høyer, M. Mosca, and A. Tapp, *Quantum Computation and Information*, 53–74 (2002).
- [45] `libs_qrem`, https://github.com/B0B01997/libs_qrem (2021).
- [46] `mthree`, <https://github.com/Qiskit-Partners/mthree> (2021).
- [47] MacBook Pro (Retina, 15-inch, Mid 2015), <https://support.apple.com/kb/SP719?> (2015).
- [48] N. J. Higham, *ACM Trans. Math. Softw.* **14**, 381–396 (1988).
- [49] W. W. Hager, *SIAM J. Sci. Stat. Comput.* **5**, 311–316 (1984).
- [50] J. Baum, M. G. Munowitz, A. N. Garroway, and A. Pines, *Journal of Chemical Physics* **83**, 2015 (1985).
- [51] M. Gärttner, J. G. Bohnet, A. Safavi-Naini, M. L. Wall, J. J. Bollinger, and A. M. Rey, *Nature Physics* **13**, 781–786 (2017).

Appendix A: Program Units Used in the Proposed Methods

The pseudo-code of step 1 in the proposed QREM methods is given by Algorithm 1. This is the most time-consuming step with $O(n|S|^2)$ time and $O(|S|^2)$ memory to the number of qubit n and the dimension of the reduced calibration matrix $|S|$ for the subspace $S \subseteq \{0, 1\}^n$. For $|S|$, we can practically assume $|S| = s$ for shot count s .

Algorithm 1 Computation of A^{-1}

Require: m local calibration matrices $A^{(0)}, \dots, A^{(m-1)}$ for arbitrary qubit blocks, noisy probability vector y with subspace S
Ensure: inverse matrix $(A^{-1})_S$ reduced into the subspace S
reduction_table \leftarrow 2d list sized $(|S|, m)$
for bitstring s in S **do**
 for calibration matrix $A^{(k)}$ in $\{A^{(0)}, \dots, A^{(m-1)}\}$ **do**
 reduction_table[s, k] \leftarrow s 's index in the subspace of $A^{(k)}$
 end for
end for
for target state bitstring t in S **do**
 for source state bitstring s in S **do**
 product $p \leftarrow 1$
 for calibration matrix $A^{(k)}$ in $\{A^{(0)}, \dots, A^{(m-1)}\}$ **do**
 index $i \leftarrow$ *reduction_table*[t, k]
 index $j \leftarrow$ *reduction_table*[s, k]
 $p \leftarrow p \cdot A_{i,j}^k$
 end for
 $[(A^{-1})_S]_{ij} \leftarrow p$
 end for
end for
return c

Next, Algorithm 2 shows the method of finding the nearest physically appropriate probability distribution by Smolin, Gambetta, and Smith [32], which is used at step 3 in the proposed methods. Our implementation adopts the priority queue to maintain all the elements of frequency distribution \hat{x} in the subspace S . Hence the time complexity of the following pseudo-code is $O(|S| \log |S|)$.

Algorithm 2 Negativity Cancellation by Smolin, Gambetta, and Smith [32] (sgs_algorithm)

Require: a vector \hat{x} (satisfying $\mathbf{1}^T \hat{x} = 1$) as a dictionary mapping state bitstring to measured count
Ensure: mitigated probability vector \tilde{x}
queue \leftarrow a priority queue of (*value, state*) sorted with *value* in ascending order.
accumulator of neative values *neg* $\leftarrow 0$
for state label k in \hat{x} **do**
 if $\hat{x}_k < 0$ **then**
 queue.push(\hat{x}_k)
 end if
end for
while *queue* is not empty **do**
 if $(neg + queue.top()) / queue.size() < 0$ **then**
 neg $\leftarrow neg + queue.pop()$
 else
 break
 end if
end while
mitigated counts $\tilde{x} \leftarrow$ empty vector (dictionary)
division value of negative accumulator $d \leftarrow queue.size()$
while *queue* is not empty **do**
 $\tilde{x}_k \leftarrow \hat{x}_k + neg / queue.size()$
end while
return \tilde{x}

Appendix B: Device information of IBM Quantum Brooklyn

The circuits are executed on IBM Quantum Brooklyn by mapping the virtual circuit qubits to physical qubits with [33, 32, 25, 31, 34, 19, 39, 30, 35, 18, 45, 20, 29, 40, 17, 46, 36, 44, 21, 28, 49, 16, 47, 24, 11, 37, 43, 12, 27, 50, 15, 53, 22, 48, 4, 26, 52, 8, 38, 51, 14, 60, 42, 23, 3, 56, 7, 41, 54, 13, 59, 5, 9, 61, 2, 55, 6, 64, 10, 58, 57, 62, 1, 63, 0] as shown in Fig. 7. The quantum circuit with depth 10 in terms of CNOT gates is enough to prepare a 65-qubit GHZ state using all the qubits in IBM Quantum Brooklyn.

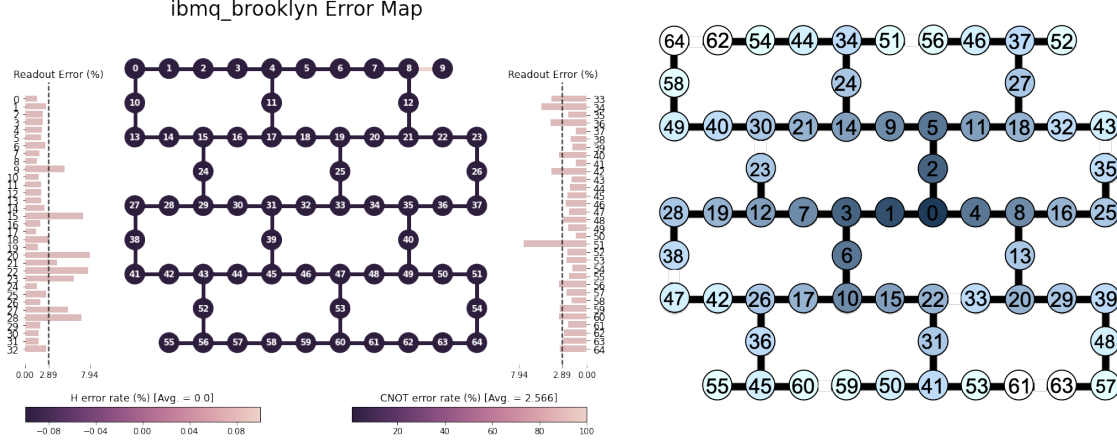


FIG. 7. The left figure shows the error map of `ibmq_brooklyn`. The numbers on the figure represent the positions of physical qubits. The right figure shows the logical qubit layout of GHZ states on `ibmq_brooklyn`. The numbers on the figure represent the positions of logical qubits. The size of GHZ states is extended in this order. The initial virtual qubits are the physical qubit “33” to “32”. In addition, qubits entangled earlier from the initial qubits are colored with darker blue, and the entangled edges of GHZ states forming the tree structure are colored black.

Appendix C: Estimation Errors of Modified Grover Algorithm

The results of numerical simulation of modified Grover algorithm under the 10-qubit system with 8192 shots and 20-qubit system with 100 shots and 8192 shots are stored here.

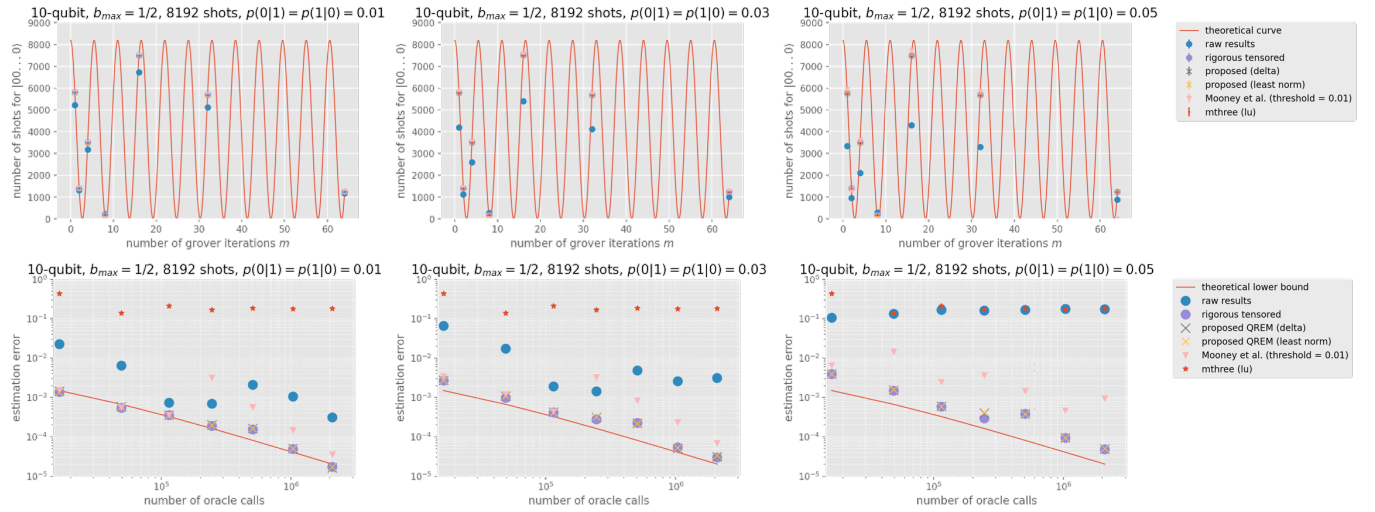


FIG. 8. The number of shots measuring $|0\rangle_{n+1}$ state and the estimation error of Monte Carlo integration on the 10-qubit system where the circuit of Grover iterators are sampled with 8192 shots. The figures in the upper row show the shot count of $|0\rangle_{n+1}$ state, and the figures in the lower row show the estimation error of Monte Carlo integration.

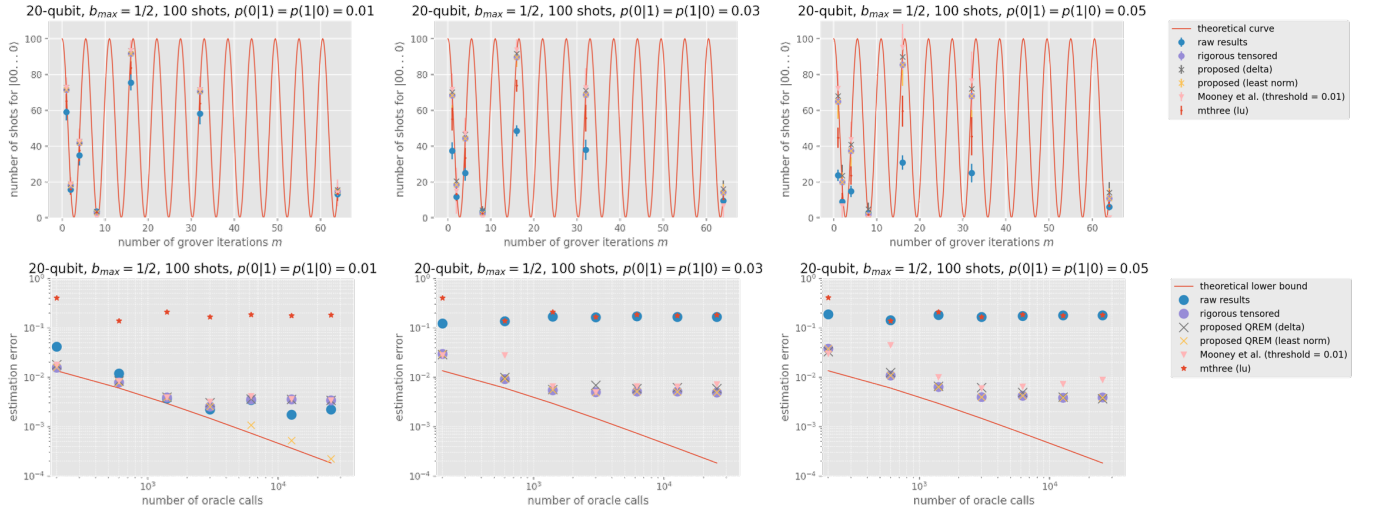


FIG. 9. The number of shots measuring $|0\rangle_{n+1}$ state and the estimation error of Monte Carlo integration on the 20-qubit system where the circuit of Grover iterators are sampled with 100 shots. The figures in the upper row show the shot count of $|0\rangle_{n+1}$ state, and the figures in the lower row show the estimation error of Monte Carlo integration.

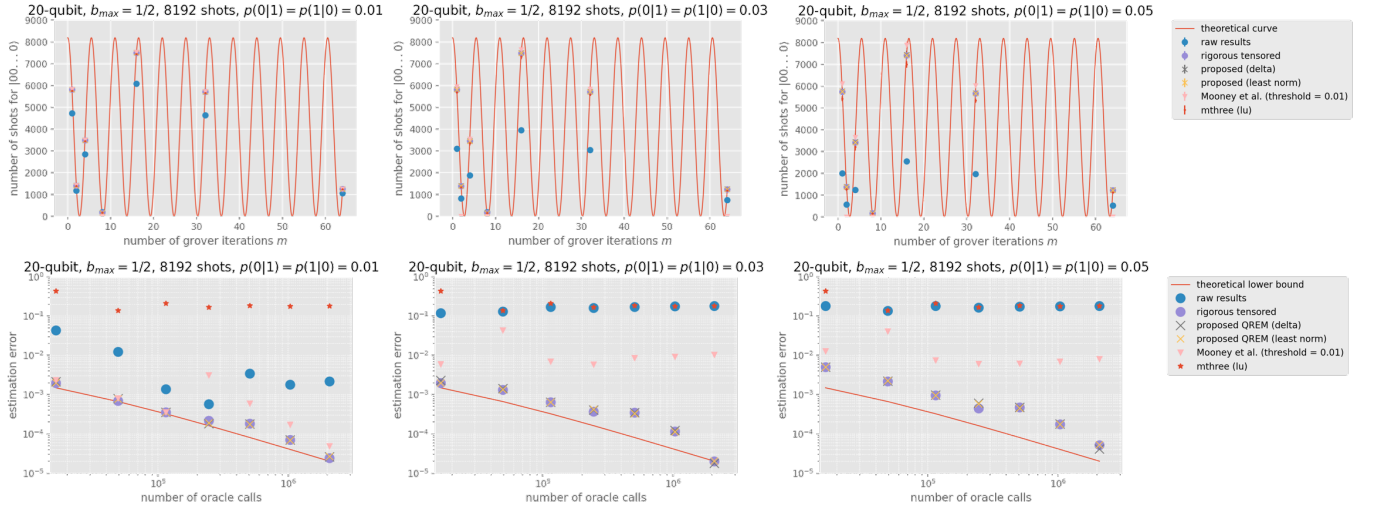


FIG. 10. The number of shots measuring $|0\rangle_{n+1}$ state and the estimation error of Monte Carlo integration on the 20-qubit system where the circuit of Grover iterators are sampled with 8192 shots. The figures in the upper row show the shot count of $|0\rangle_{n+1}$ state, and the figures in the lower row show the estimation error of Monte Carlo integration.

For all of these settings in Fig. 8, 9, and 10, the proposed QREM methods exhibit the best estimation accuracy among other efficient QREM methods [27, 28]. The estimation errors by the proposed methods are closest to the plots mitigated by the exponential-time rigorous matrix inversion method.